IIETA International Information and Engineering Technology Association
Advancing the World of Information and Engineering

Traitement du Signal
Vol. 40, No. 3, June, 2023, pp. 1153-1161
Journal homepage: http://iieta.org/journals/ts

An Integrative Approach for Mineral Nutrient Quantification in Dioscorea Leaves: Uniting Image Processing and Machine Learning

Yufei Song, Xi Meng, Yan Li, Zhiguo Liu, Huitao Zhang*

College of Future Information Technology, Shijiazhuang University, Shijiazhuang 050035, China

Corresponding Author Email: 1102209@sjzc.edu.cn

https://doi.org/10.18280/ts.400331

Received: 20 February 2023
Accepted: 16 May 2023

Keywords:
Dioscorea, nutrient, image processing, machine learning

ABSTRACT

Dioscorea, lauded for its environmental sustainability and versatility, is pivotal in various industries, ranging from food to medicine. The significant yields it offers, coupled with low cultivation inputs and substantial nutritional benefits - including high protein content and minimal sugar levels, necessitate precision in yield predictions and growth management. This, in turn, fosters the evolution of mechanized agriculture and automation. To address this need, a novel methodology amalgamating digital image processing and machine learning algorithms has been established to accurately determine the mineral nutrient content in Dioscorea leaves. This methodology initiates with the separation of the foreground and background in leaf images, achieved through the implementation of the H-component OTSU algorithm. Subsequently, the computation of 54 color features is carried out, and machine learning techniques are harnessed to form models that delineate image features in correlation with a SPAD value exceeding 0.9. The aspiration of this model development lies in the prediction of chlorophyll, nitrogen, phosphorus, and potassium content in Dioscorea leaves. It has been determined that the Multilayer Perceptron (MLP), post 100 iterations, constructs the most accurate model for predicting SPAD content in Dioscorea nipponica. In terms of nitrogen content prediction, a regression model exploiting the SL characteristic has been discovered to be optimal, demonstrating an R2 of 0.850. For phosphorus, a model incorporating the NRI characteristic has yielded an R2 of 0.819, affirming its efficacy. Meanwhile, potassium content prediction has been found to be most precise with a model centered on the Sb characteristic, as evidenced by an achieved R2 of 0.865. This cutting-edge methodology can significantly advance the agricultural sector, particularly in the realm of mechanized agriculture and automation.

1. INTRODUCTION

A reliable estimation of mineral nutrient content during Dioscorea growth is a fundamental prerequisite for applying sound and rational fertilization strategies. In today's agricultural production and precision agriculture, the urgency of prompt, non-destructive diagnosis, and estimation of crop growth has emerged as a pressing issue [1, 2]. Although chemical analysis is the prevalent method due to its accuracy, and also forms the basis for various extended methods, it is characterized by its complexity, time-consuming nature, and potential for environmental pollution caused by the use of reagents [3].

Current research on harnessing digital image technology for crop mineral nutrient detection primarily focuses on leaf scale, due to its lower susceptibility to interference factors such as soil, background, and measurement environment, leading to comparatively ideal color feature data. Examining the correlation between leaf scale image features and mineral nutrient content provides insights into the biological significance between digital image color features and crop nutrient absorption, laying a theoretical and methodological foundation for crop mineral nutrient content detection via close-range, non-contact measurement methods [3].

Technologically advanced tools and methods, including ground object spectrometers and hyperspectral imaging devices, have been exploited for detecting crop physiological status and growth information. These devices, however, are expensive and necessitate professional operators for sampling. It has been found that the first two bands of spectral data, most sensitive to the mineral nutrient content of crops, are within the visible light region. This discovery implies that digital images captured in the visible light range could present a cost-effective and user-friendly solution for assessing the mineral nutrient status of field crops [4].

Chlorophyll content of rice leaves was assessed using a narrowband dual camera system, and a strong correlation was found between the Leaf Greenness Index and the chlorophyll content of rice leaves [4]. Evidence from previous studies indicates that the mathematical processing and combination of basic image features, particularly color features, yield structural parameters that demonstrate a stronger correlation with the mineral nutrients, particularly nitrogen content, of the crop [5]. Indices such as (G-R), G/R, NGI, NRI, and hue index were utilized to estimate rice biomass, nitrogen content, and leaf area index (LAI), revealing that the (G-R) and G/R indices surpassed other indicators in their estimations [6]. However, a single green component in the RGB color space was found insufficient for accurately representing vegetation greenness, as changes in the values of the red and blue components can also influence the perceived greenness [7]. A dark green index (DGCI) was introduced based on the HSI color space, and it

was found to correlate strongly with crop nitrogen content [8]. Studies exploring the relationship between various color components in the RGB color space and chlorophyll content in wheat and rye leaves under different field environment weather conditions found that the indicators (R-B)/(R+B) correlated strongly with leaf chlorophyll content under varying weather conditions [9].

Moreover, leaf color indicators sensitive to nitrogen content in wheat during the two stages of turning green and jointing were investigated, with the best correlation found between the turning green period and plant nitrogen content, and color feature indicators G/R and NRI [10]. A mobile app was developed to collect images of corn leaves through contact photography, and correlation analysis with chlorophyll values was conducted. Models were established using stepwise regression and neural networks, with R2 and RMSE of 0.74 and 6.2 for the stepwise regression model, and 0.82 and 5.1 for the neural network model, respectively [3]. Ordinary digital cameras were used to directly collect wheat images in the field, and 12 statistical features of RGB color space were extracted as image evaluation indicators. A neural network model was established for predicting nitrogen content in wheat leaves, indicating that the neural network algorithm outperformed other univariate regression methods [11, 12].

Digital images of sesame seeds were collected and 12 color indicators were extracted from RGB and Lab color spaces. A correlation analysis was conducted between these color indicators and chlorophyll content, and a random forest prediction model was established, yielding an R2 of 0.9 [13].

In summation, the field of crop mineral nutrition assessment based on imaging has predominantly witnessed researchers focusing on the relational model between a single nutrient element and crop growth status. Yet, research on constructing a prediction model for multiple mineral nutrients in crops is not as extensive. In this study, a combination of digital image processing technology and machine learning technology is utilized to construct prediction models correlating leaf image information with SPAD, nitrogen, phosphorus, and potassium elements of Dioscorea plants. The intent of this study is to employ digital images and machine learning technology to formulate a prediction model for multiple mineral nutrients of Dioscorea.

2. MATERIAL AND METHOD

2.1 Acquisition of images and determination of mineral nutrient element content

This study was executed in a field located at Songgang Village, Nanzhuang Town, Li County, Baoding City, Hebei Province, China, within the Hebei Agricultural University premises. The subject of the investigation was yam, grown in sandy loam soil with basic physiochemical properties, including organic matter (7.51 g/kg), NH4'-N (2.24 mg/kg), NO-N (6.81 mg/kg), alkali-hydrolyzed nitrogen (29.05 mg/kg), available phosphorus (7.08 mg/kg), and available potassium (65.88 mg/kg). Fertilizers such as urea (N46%), superphosphate (P; 0; 12%), and potassium sulfate (K; 0; 50%) were tested with 12 distinct fertilization levels, applying conventional fertilization management practices. The application of nitrogen fertilizer was split into a 3:7 base-to-topdressing ratio, while the entire phosphorus fertilizer was applied once, and potassium fertilizer was applied in a 4:6 base-to-topdressing ratio. The experimental design followed a randomized complete block, and each plot measured $2.1 \times 4 = 8.4$ m, with each treatment replicated thrice, totaling 36 plots. Samples were collected on September 27, 2017, with eight leaves randomly chosen from each plot. After discarding incomplete leaves, 259 leaves were procured, stored in a container with an ice pack, and swiftly transported to the laboratory. Images were captured using a Sony FDR-XP35 4K high-definition camera under laboratory fluorescent lighting conditions. Post image acquisition, a SPAD-502PLUS portable chlorophyll meter (Minolta Camera Co., Osaka, Japan) was used to determine chlorophyll content in the leaves. Based on their SPAD values, Dioscorea plant leaves were categorized into six groups for nitrogen content determination, with ranges of [0,10), [10,20), [20,30), [30,40), [40,50), and [50,60), reflecting a many-to-one relationship between color characteristics and nitrogen content. Nitrogen, phosphorus, and potassium content in the leaves were subsequently determined using chemical reagent methods. All images were preserved in JPG format, and representative images from the experiment are illustrated in Figure 1.

2.2 Feature extraction

2.2.1 Target extraction

The OTSU method, also known as the maximum inter-class variance algorithm, employs clustering principles to segment image grayscale into two parts based on grayscale levels. This segmentation is achieved by maximizing the grayscale variance between segments while minimizing the variance within each segment. The calculation of variance helps identify an appropriate grayscale level for image segmentation. Thus, the OTSU algorithm can autonomously select thresholds for binarization during the binarization process. Regarded as an optimal threshold selection algorithm in image segmentation, the OTSU algorithm is distinguished by its simple computation and independence from image brightness and contrast. As such, the maximization of inter-class variance equates to the minimization of the probability of misclassification. The detailed process of the algorithm is outlined below.

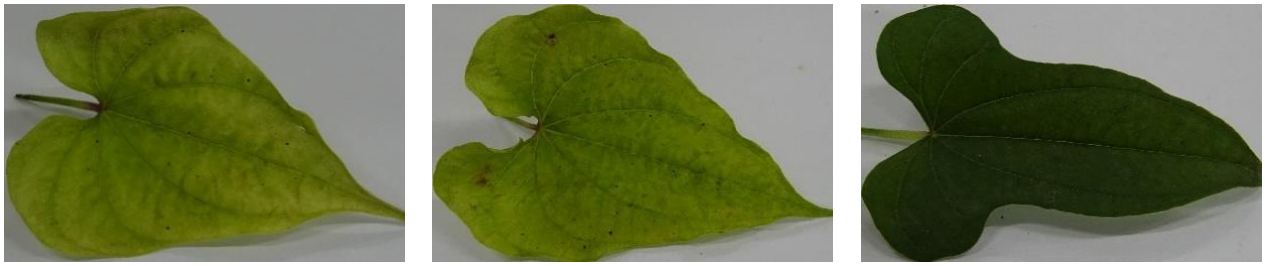

Figure 1. Image of Dioscorea leaves

Input: Original image
Output: Blade target

Step 1: Convert the image from RGB color space to HSI color space. This involves converting the red, green, and blue values into their hue, saturation, and intensity counterparts. The conversion process can be done using various programming languages and libraries, including Python, OpenCV, and NumPy.
Step 2: Define 't' as the set threshold. Here, several variables are introduced:
'w0': The proportion of foreground pixel points in the image after separation;
'u0': The average grayscale of the foreground pixels after separation;
'w1': The proportion of the number of subject pixels in the image after separation;
'u1': The average grayscale of the separated pixels in the scene.
Compute the total average grayscale of the image as 'u', calculated using the formula 'u = w0*u0 + w1*u1'.
Step 3: Iterate through the 't' from grayscale levels 'L', with the goal of maximizing the variance between the foreground and background when 't' is a certain value. This specific 't' value becomes the threshold needed. The variance 'g' can be calculated using the following formula:
'$g = w0*(u0-u)^2 + w1*(u1-u)^2$'. The goal is to find the 't' that maximizes this variance.

2.2.2 Feature extraction

The extraction of multiple features to bolster the accuracy of regression models has been well-documented by several researchers [1-3, 9, 14]. The initial images are saved in an 8-bit RGB format, a mixed color space that leaves the color features vulnerable to external environmental influences such as lighting intensity. It has been suggested that using a set of invariant moments to normalize these features can provide positive outcomes [1, 15, 16]. The subsequent normalization formula for the color features can mitigate the light's impact on the image color, as displayed in Eqns. (1)-(3).

$$r = R/\sqrt{R^2 + G^2 + B^2} \tag{1}$$

$$g = G/\sqrt{R^2 + G^2 + B^2} \tag{2}$$

$$b = B/\sqrt{R^2 + G^2 + B^2} \tag{3}$$

Invariant moments of the image were employed, yielding a set of parameters that effectively eliminated the influence of external factors such as the environment and camera type on the image color. Certain color spaces utilize saturation and brightness as encapsulations of color perception. These color spaces, which include the HSI (Hue, Saturation, Intensity) color space, the Lab* color space (operating on three axes: a=green to red; b=blue to yellow; L=brightness), and the XYZ color space, have been employed to reduce the effect of light brightness on color. Eqns. (4)-(7) illustrate the conversion of RGB images to HSI, XYZ, and Lab* color spaces.

$$H = \begin{cases} \theta & (G \geq B) \\ 2\pi - \theta & (G < B) \end{cases} \tag{4}$$

where, $\theta = arccos\left\{\frac{[(R-G)+(R-B)]/2}{[(R-G)^2+(R-B)(B-G)]^{1/2}}\right\}$

$$S = 1 - 3/(R+G+B) \cdot min(R,G,B) \tag{5}$$

$$I = (R+G+B)/3 \tag{6}$$

$$\begin{cases} R_1 = gamma(\frac{R}{255.0}) \\ G_1 = gamma(\frac{G}{255.0}) \\ B_1 = gamma(\frac{B}{255.0}) \end{cases} \tag{7}$$

where, $gamma(x) = \begin{cases} \left(\frac{x+0.055}{1.055}\right)^{2.4} & (x > 0.04045) \\ \frac{x}{12.92} & (otherwise) \end{cases}$

$$\begin{bmatrix} X \\ Y \\ Z \end{bmatrix} = \begin{bmatrix} 0.4124 & 0.3576 & 0.1805 \\ 0.2126 & 0.7152 & 0.0722 \\ 0.0193 & 0.1192 & 0.9505 \end{bmatrix} * \begin{bmatrix} R_1 \\ G_1 \\ B_1 \end{bmatrix} \tag{8}$$

$$L = \begin{cases} 116 \times f(Y/Y_n) - 16.0; if\ Y/Y_n > 0.008856 \\ 903.3 \times (Y/Y_n); \quad if\ Y/Y_n \leq 0.008856 \end{cases} \tag{9}$$

$$a^* = 500[f(X/X_n) - f(Y/Y_n)] \tag{10}$$

$$b^* = 200[f(Y/Y_n) - f(Z/Z_n)] \tag{11}$$

where, $f(t) = \begin{cases} 1/3\left(\frac{6}{29}\right)^3 t + 4/29, if\ t \leq 0.008856 \\ t^{\frac{1}{3}} \quad if\ t > 0.008856 \end{cases}$

and X_n, Y_n, Z_n describe a specified white object-color stimulus.

An average of all pixels across three color spaces in the target image was employed as a corresponding color evaluation indicator for the image. In this context, mean values of RGB mode images are denoted as R, G, and B respectively. Similarly, mean values for HSI and Lab* mode images are denoted as H, S, I, L, a*, and b* respectively. The formula to calculate the image mean index, denoted as μ, is presented in Eq. (12):

$$\mu = \frac{1}{MN}\sum_{i=1}^{M}\sum_{j=1}^{N} P(i,j) \tag{12}$$

where, M and N represent the rows and columns of effective pixels in the target image, and $P(i,j)$ represents the color grayscale value of the effective pixels.

In the realm of image analysis, a rise in color difference amongst effective pixels in an image corresponds to an increase in standard deviation for the same image feature. Thus, the standard deviation of the color of effective pixels has been utilized as an index of significance, as shown in Eq. (13).

$$\sigma = \sqrt{1/MN\sum_{i=1}^{M}\sum_{j=1}^{N}[P(i,j) - \mu]^2} \tag{13}$$

Innovative indicators, derived from interactive processing or arithmetic combinations of basic color indicators, exhibit a more stable and closely related relationship with the

chlorophyll content in plant leaves [1]. Previous literature [17-21] and multiple experimental studies have facilitated the selection of a combined set of indicators for the detection of mineral nutrient content in wheat, namely: R-G, R+B, R-G-B, R+G-B, NRI, NBI, NGI, and DGCI. The corresponding formulas are shown in Eqns. (14)-(17).

$$NRI = \frac{R}{R+G+B} \tag{14}$$

$$NGI = \frac{G}{R+G+B} \tag{15}$$

$$NBI = \frac{B}{R+G+B} \tag{16}$$

$$DGCI = \frac{(H-60)/60 + (1-S) + (1-I)}{3} \tag{17}$$

2.3 Analysis of modeling approaches

2.3.1 Regression via XGBoost

The employment of the XGBoost algorithm, a sophisticated version of the gradient boosting algorithm, has been evidenced as enhancing the realm of plant nutrient diagnosis through image analysis. In contrast to parallel computing algorithms like random forests, XGBoost implements a sequential operation, constructing and evaluating trees one after another. This approach enables a detailed and precise model to be built, augmenting the accuracy of plant nutrient diagnoses. The gradient boosting algorithm has applications in both regression and classification problems, and it should be noted that the internal decision tree utilized by XGBoost is a regression tree.

2.3.2 Regression via K-Nearest Neighbor (KNN)

The KNN algorithm, a relatively uncomplicated machine learning method, is versatile enough to handle both classification and regression tasks. In the context of image-based plant nutrient diagnosis, the algorithm can classify or predict plant nutrient statuses based on color features extracted from images. In classification, the nutrient status of a plant is determined by the most frequently occurring nutrient status amongst its k-nearest neighbors in the feature space. For regression problems, the mean nutrient content of its k-nearest neighbors is used to predict the plant's nutrient content. This approach enhances the accuracy and efficiency of plant nutrient status diagnoses, improving the efficacy of nutrient management strategies.

2.3.3 Regression via Lasso

The Lasso method, also known as the Least Absolute Selection and Shrinkage Operator, applies a shrinkage estimation technique that compacts variable coefficients and sets specific regression coefficients to zero through the construction of a penalty function. This technique results in variable selection and mitigates the overfitting problem commonly associated with standard linear regression. In image-based plant nutrient diagnosis, Lasso regression can be deployed to select the most significant color features from images for the prediction of plant nutrient status. By reducing the coefficients of less relevant features to zero, Lasso regression effectively diminishes the feature space's dimensionality and prevents overfitting, which in turn, improves the model's generalizability and predictive accuracy.

2.3.4 Regression via Multilayer Perceptron (MLP)

MLP, also referred to as an Artificial Neural Network (ANN), is a type of neural network characterized by the potential to incorporate multiple hidden layers, in addition to input and output layers. In an MLP, complete connectivity is maintained between layers, with the lowermost layer serving as the input layer, the middle layers functioning as hidden layers, and the final layer acting as the output layer. Within the context of image-based plant nutrient diagnosis, MLP can be employed to discern intricate patterns in color features extracted from images for predicting plant nutrient status. The input layer receives the color features, the hidden layers learn and represent the intricate relationships between these features and the nutrient status, and the output layer provides the predicted nutrient status. By learning these complex patterns, MLP effectively models the non-linear relationships between color features and nutrient status, enhancing the predictive accuracy of the model.

3. RESULTS

3.1 Image segmentation and feature extraction

The conducted study presented significant strides in the field of image segmentation and feature extraction. Firstly, an implementation of the OTSU algorithm was necessitated to cluster grayscale levels within an image. A grayscale histogram was calculated for the image, which displayed Dioscorea leaves under laboratory conditions. The challenging lighting conditions and nebulous background rendered shadow segmentation at the junction of foreground and background in the RGB image challenging. As a result, an extraction of the H component histogram from the image was performed and subsequent analysis of its peak changes was undertaken. It was concluded that segmentation was more feasible within the H component, a finding illustrated in Figure 2. Figure 3 presents the H-component grayscale image of the Dioscorea leaves. The results of the target extraction in relation to the image in Figure 1, post feature extraction process per Section 2.2, are displayed in Figure 4.

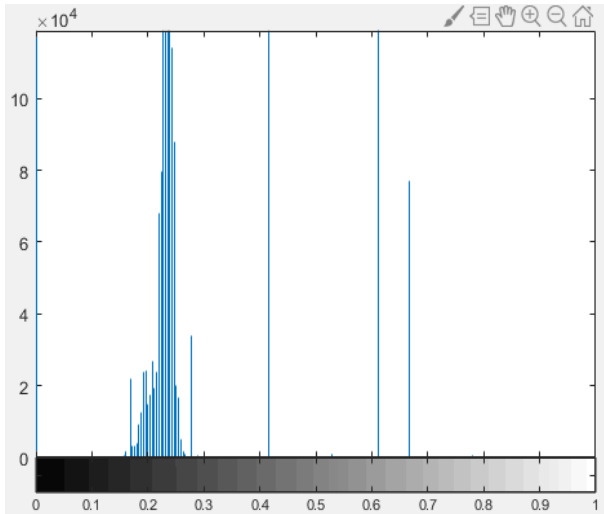

Figure 2. H-component grayscale histogram of leaves of Dioscorea

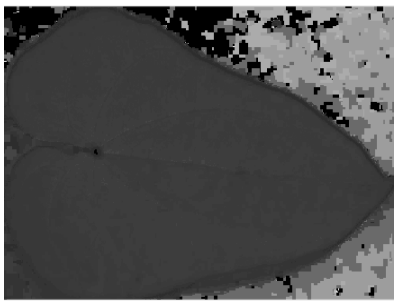

Figure 3. H-component grayscale image of Dioscorea leaves

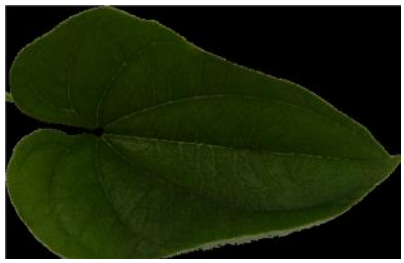

Figure 4. Extracted Dioscorea leaves

The research assumed the existence of two pixel types in images: foreground pixels and background pixels, and the bimodal nature of the histogram was assumed. An optimal threshold for separating these two pixel types was determined through the intra-class variance method or the equivalent inter-class variance. The H-component OTSU was used to segment the Dioscorea leaves, whereby the RGB image was converted into HIS space representation. Following this, the H component was extracted for image segmentation, and the segmented image was reconverted into RGB space representation (Figure 4).

3.2 Correlation analysis between color features and SPAD

Following this, an analysis of the correlation between color features and SPAD was conducted. First-order distance and second-order moments were extracted from RGB, HSI, XYZ, and Lab color spaces, giving rise to 54 color feature combinations, which included NRI, NGI, NBI, DGCI, among others. Table 1 details the correlation analysis between image feature values and SPAD. It was observed that the majority of color features exhibited a strong correlation with SPAD. The correlation between RGB space-normalized color features and SPAD surpassed that of color features without normalization operations, indicating that normalization can effectively mitigate light influence to some extent. Simultaneously, the eigenvalues of HIS space and Lab space demonstrated a strong correlation with SPAD. The correlation between color feature combinations and SPAD values was higher than that of single variables, suggesting that non-linear combinations between features can give a more accurate representation of leaf chlorophyll content.

Table 1. Correlation analysis between image feature values and SPAD

Features	Correlation	Features	Correlation	Features	Correlation
R	**-0.956**	L	**-0.952**	G-B	**-0.952**
G	**-0.946**	a*	0.429	R+G-B	**-0.967**
B	0.427	b*	**-0.961**	G/R	0.873
SR	0.407	SL	0.712	G/B	-0.640
SG	0.576	Sa*	0.022	(R-B)/(R+B) (R-G)/(R+G)	-0.853
SB	0.530	Sb*	-0.134	(R-G)/(R+G)	-0.869
r	**-0.933**	X	**-0.948**	(G-B)/(G+B)	-0.790
g	0.754	Y	**-0.962**	(R-B)/(R+G+B)	**-0.935**
b	0.795	Z	-0.896	(R-G)/(R+G+B)	-0.792
Sr	0.814	SX	**-0.952**	(G-B)/(R+G+B)	-0.581
Sg	0.898	SY	-0.429	r-g-b	**-0.978**
Sb	0.813	SZ	**-0.961**	r-g	-0.878
H	**0.973**	R-G-B	-0.482	r-b	**-0.952**
S	-0.798	R-G	-0.126	g/r	**-0.900**
I	**-0.938**	R-B	**-0.977**	NRI	**-0.976**
SH	**0.973**	R+G	**-0.957**	NGI	0.012
SS	0.823	R+B	**-0.902**	NBI	0.819
SI	0.711	G+B	**-0.909**	DGCI	**0.940**

3.3 Color features and SPAD modeling results

In this study, regression models for eigenvalues and SPAD were created using XGBoost, KNN, Lasso, and MLP algorithms. Nested cross-validation was employed due to the limited number of model samples and the significant issue of multicollinearity. The 10-fold outer cross-validation divided samples into 10 subsets for model performance evaluation (181/78, 182/77), while grid search was used for parameter optimization in the 10-fold inner cross-validation. The predicted results of each model, after 100 iterations, are given in Table 2, with the optimal prediction model result from MLP shown in Figure 5.

The coefficients in these models symbolize the importance of the corresponding color features in predicting the nutrient status of plants. A larger coefficient indicates a stronger relationship between the color feature and the nutrient status. Therefore, the coefficients can offer insights into which color features are most indicative of the nutrient status, thereby guiding future studies in the feature extraction process.

Table 2. Evaluation of prediction results of each model

Model	R^2	RMSE
XGBoost	0.978	2.505
KNN	0.955	3.623
Lasso	0.982	2.27
MLP	0.984	2.155

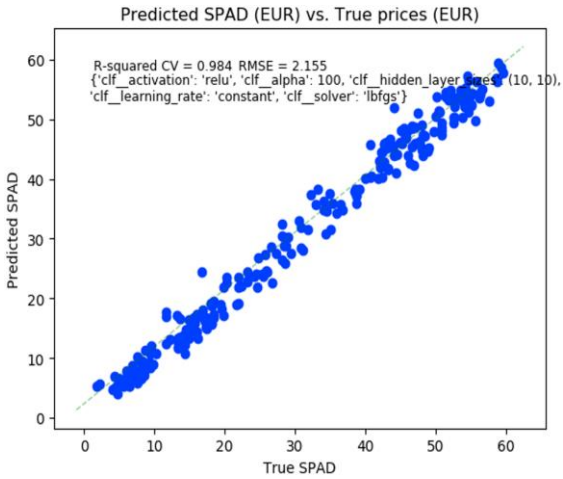

Figure 5. The optimal prediction model result

The results indicate that the MLP model surpasses other models in terms of prediction accuracy, as displayed in Figure 5. This suggests that MLP can effectively learn complex, non-linear relationships between color features and the nutrient status. However, these findings require further validation, and additional research is necessary to explore the potential of other machine learning algorithms in diagnosing plant nutrient status.

3.4 Correlation analysis and modeling results between color features and N content

In the current research, leaves from Dioscorea species were allocated into six categories based on their SPAD values to measure nitrogen content. Categories were established as [0,10), [10,20), [20,30), [30,40), [40,50), and [50,60), forming a matrix of 55*6 dimensions to capture nitrogen content against 54 eigenvalues, thus positing a many-to-one relationship between color features and nitrogen content.

Table 3 showcases a moderate correlation between image color features and nitrogen content, although inferior to the correlation between color features and SPAD content. Lack of cross-validation due to restricted sample size necessitated the use of SL as a variable in the model given its robust correlation with nitrogen content. The developed model (N=0.934+0.002SL) yielded an adjusted R-square of 0.850, indicating that 85% of the variance in nitrogen content could be explained by this model.

The coefficients, representative of the relevance of corresponding color features in nitrogen content prediction, highlight that larger coefficients symbolize stronger relationships. Thus, the coefficient values can guide future studies in selecting influential color features to predict nitrogen content. However, the study emphasizes the need for further investigation to validate the model and explore additional machine learning techniques for plant nutrient diagnosis.

In considering the relationship between original RGB color features and nitrogen content, the correlation is not highly significant. Nonetheless, the SR second-order moment of the red component has a positive correlation with nitrogen content, represented by a correlation coefficient of 0.921. The XYZ color space, when evaluated from the perspective of color space, exhibits the highest correlation with leaf nitrogen content. Features X and Z, and leaf nitrogen content display a correlation exceeding 0.9. Similarly, correlation surpasses 0.9 between Sr, H, SH, SL, and leaf nitrogen content, with SL exhibiting the most potent correlation at 0.938.

Thus, the current study establishes a strong correlation between several color features and nitrogen content, offering insights for future studies and machine learning applications. However, it also underscores the need for expanded research, particularly with larger sample sizes and diverse algorithms to better understand and validate these relationships.

Table 3. Correlation analysis between image feature values and N

Features	Correlation	Features	Correlation	Features	Correlation
R	-0.898	L	-0.875	G-B	-0.828
G	-0.868	a*	0.293	R+G-B	-0.872
B	0.259	b*	-0.869	G/R	0.844
SR	**0.921**	SL	**0.938**	G/B	-0.361
SG	0.893	Sa*	-0.247	(R-B)/(R+B) (R-G)/(R+G)	-0.667
SB	0.386	Sb*	0.008	(R-G)/(R+G)	-0.857
r	-0.893	X	**-0.905**	(G-B)/(G+B)	-0.612
g	0.781	Y	-0.894	(R-B)/(R+G+B)	-0.784
b	0.636	Z	**-0.901**	(R-G)/(R+G+B)	-0.808
Sr	**0.917**	SX	-0.875	(G-B)/(R+G+B)	-0.409
Sg	0.840	SY	-0.293	r-g-b	-0.872
Sb	0.628	SZ	-0.869	r-g	-0.865
H	**0.914**	R-G-B	-0.841	r-b	-0.820
S	-0.632	R-G	-0.338	g/r	-0.862
I	-0.898	R-B	-0.875	NRI	-0.874
SH	**0.914**	R+G	-0.887	NGI	0.148
SS	0.660	R+B	**-0.903**	NBI	0.648
SI	0.875	G+B	-0.898	DGCI	0.899

3.5 Correlation analysis and modeling results between color features and P content

In the investigation into the association between color features and phosphorus (P) content, the findings disclosed in Table 4 demonstrate notable similarities to the correlations between color features and nitrogen content. Specifically, nine features were identified, each possessing a significant correlation coefficient (|R|) exceeding 0.9.

A distinction was noticed in the association between the green (G) component in the initial RGB color space and the leaf phosphorus content when contrasted with the nitrogen

content in the leaves, with a correlation of 0.9 being attained. The HSI color space was shown to hold the highest correlation with leaf phosphorus content from a color space perspective. Interestingly, the association between combination features and leaf phosphorus content exceeded the average correlation of the color space.

The most considerable correlation with leaf phosphorus content was shown by the following features: G, H, SH, L, SX, R-B, R+G-B, r-g-b, and the Normalized Difference Vegetation Index (NRI). This aligns with the findings of the correlation analysis of color and fabric structure presented in the study by NUMBER:1 [1].

In Table 4, the Normalized Difference Vegetation Index (NRI), due to its highest correlation with P content, was selected for modeling. An adjusted R-squared (adjR^2) of 0.819 was achieved, reflecting a robust model fit. The model equation was formulated as:

$$P = 2.029 - 1.928NRI \quad (18)$$

Table 4. Correlation analysis between image feature values and P

Features	Correlation	Features	Correlation	Features	Correlation
R	-0.891	L	**-0.900**	G-B	-0.896
G	**-0.900**	a*	0.467	R+G-B	**-0.905**
B	0.521	b*	-0.894	G/R	0.878
SR	0.487	SL	0.711	G/B	-0.735
SG	0.585	Sa*	-0.040	(R-B)/(R+B) (R-G)/(R+G)	-0.786
SB	0.639	Sb*	0.411	(R-G)/(R+G)	-0.860
r	-0.898	X	-0.880	(G-B)/(G+B)	-0.729
g	0.764	Y	-0.894	(R-B)/(R+G+B)	-0.863
b	0.717	Z	-0.844	(R-G)/(R+G+B)	-0.796
Sr	0.886	SX	**-0.900**	(G-B)/(R+G+B)	-0.519
Sg	0.850	SY	-0.468	r-g-b	**-0.914**
Sb	0.834	SZ	-0.894	r-g	-0.861
H	**0.906**	R-G-B	-0.883	r-b	-0.875
S	-0.725	R-G	-0.140	g/r	-0.893
I	-0.889	R-B	**-0.908**	NRI	**-0.925**
SH	**0.906**	R+G	-0.899	NGI	0.049
SS	0.730	R+B	-0.852	NBI	0.745
SI	0.799	G+B	-0.886	DGCI	0.889

Table 5. Correlation analysis between image feature values and K

Features	Correlation	Features	Correlation	Features	Correlation
R	-0.667	L	-0.766	G-B	-0.834
G	-0.772	a*	0.843	R+G-B	-0.762
B	0.882	b*	-0.796	G/R	0.544
SR	0.244	SL	0.469	G/B	-0.877
SG	0.267	Sa*	-0.025	(R-B)/(R+B) (R-G)/(R+G)	-0.786
SB	**0.901**	Sb*	-0.784	(R-G)/(R+G)	**-0.943**
r	-0.624	X	-0.626	(G-B)/(G+B)	-0.514
g	0.331	Y	-0.672	(R-B)/(R+G+B)	**-0.936**
b	**0.923**	Z	-0.545	(R-G)/(R+G+B)	**-0.906**
Sr	0.609	SX	-0.766	(G-B)/(R+G+B)	-0.386
Sg	0.851	SY	-0.843	r-g-b	-0.818
Sb	**0.944**	SZ	-0.796	r-g	-0.521
H	0.730	R-G-B	-0.527	r-b	-0.883
S	**-0.929**	R-G	0.407	g/r	0.586
I	-0.674	R-B	-0.753	NRI	-0.790
SH	0.730	R+G	-0.722	NGI	0.492
SS	**0.922**	R+B	-0.555	NBI	**0.933**
SI	0.752	G+B	-0.682	DGCI	0.677

3.6 Correlation analysis and modeling results between color features and K content

Presented in Table 5 are the Pearson correlation coefficients between the image attributes and the potassium (K) content. It was discovered that the association between leaf potassium content and color attributes exhibits a greater value, exceeding 0.9, when compared to the correlations with nitrogen (N) and phosphorus (P). While the quantity of color attributes remains consistent, the highest absolute correlation coefficient (|R|max), standing at 0.944, is noticed between the Sb and leaf K content.

Differing from the correlations with nitrogen and phosphorus, it was predominantly combination attributes such as (R-G)/(R+G), (R-B)/(R+G+B), (R-G)/(R+G+B), and NBI that manifested a stronger association with potassium. When analyzed from the perspective of color space, the best correlation with leaf potassium content was shown by RGB and HSI color spaces.

Building upon the highest correlation with K content,

modeling was carried out using Sb. This model yielded an adjR2 of 0.865, formulated by the following equation:

$$K = 1.249 - 0.021Sb \quad (19)$$

4. CONCLUSIONS

The utilization of digital image processing technology and machine learning methodologies was explored in this study, with the primary objective of extracting targeted images of Dioscorea leaves. A total of 54 color feature values were computed using RGB, HSI, XYZ, and Lab color spaces. The established correlations between these color features and SPAD values, alongside nitrogen (N), phosphorus (P), and potassium (K) content in Dioscorea leaves were evaluated.

It has been deduced from the findings that:

(1) Chlorophyll content in Dioscorea leaves can be predicted effectively using digital image technology and machine learning methodologies. This offers a robust foundation for non-destructive testing of Dioscorea leaves. In the arena of nutrient content prediction, the MLP model showed superior performance compared to other tested methods, such as KNN, XGBoost, and Lasso.

(2) A significant correlation was observed between color features and mineral nutrients. The process of normalization appears to diminish the influence of light on leaf characteristics, with the normalized RGB color space demonstrating a higher correlation with mineral nutrients than unnormalized color features.

(3) Combining color features produced a higher correlation with mineral nutrient content in Dioscorea leaves than a single variable. This suggests that a non-linear combination of features provides a more comprehensive understanding of the chlorophyll content in Dioscorea leaves. It paves the way for future research into the construction of additional image color features to enhance the evaluation of crop nutrient content.

(4) It should be noted that this study was conducted in a controlled laboratory environment. Therefore, future research should include the collection of leaf images in field prototypes, paving the way towards non-destructive and rapid detection of Dioscorea leaves.

FUNDING

This paper was supported by Scientific Science and Technology Research Projects of Universities in Hebei (Grant No.: QN2021409) and China University Industry, University and Research Innovation Fund (Grant No.: 2021ITA05004).

REFERENCES

[1] Song, Y., Teng, G., Yuan, Y., Liu, T., Sun, Z. (2021). Assessment of wheat chlorophyll content by the multiple linear regression of leaf image features. Information Processing in Agriculture, 8(2):232-243. https://doi.org/10.1016/j.inpa.2020.05.002

[2] Song, Y., Li, S., Liu, Z., Zhang, Y., & Shen, N. (2022). Analysis on chlorophyll diagnosis of wheat leaves based on digital image processing and feature selection. Traitement du Signal, 39(1):381-387. https://doi.org/10.1 8280/ts.390140

[3] Vesali, F., Omid, M., Kaleita, A., Mobli, H. (2015). Development of an android app to estimate chlorophyll content of corn leaves based on contact imaging. Computers and Electronics in Agriculture, 116: 211-220. https://doi.org/10.1016/j.compag.2015.06.012

[4] Shibayama, M., Sakamoto, T., Takada, E., Inoue, A., Morita, K., Yamaguchi, T., Takahashi, W., Kimura, A. (2012). Estimating rice leaf greenness (SPAD) using fixed-point continuous observations of visible red and near infrared narrow-band digital images. Plant Production Science, 15(4): 293-309. https://doi.org/10.1626/pps.15.293

[5] Chen, J., Yao, X., Huang, F., Liu, Y., Yu, Q., Wang, N., Xu, H., Zhu, Y. (2016). N status monitoring model in winter wheat based on image processing. Transactions of the Chinese Society of Agricultural Engineering, 32(4): 163-170.

[6] Wang, Y., Wang, D., Zhang, G., Wang, J. (2013). Estimating nitrogen status of rice using the image segmentation of GR thresholding method. Field Crops Research, 149: 33-39. https://doi.org/10.1016/j.fcr.2013.04.007

[7] Richardson, M.D., Karcher, D.E., Purcell, L. C. (2001). Quantifying turfgrass cover using digital image analysis. Crop Science, 41(6), 1884-1888. https://doi.org/10.2135/cropsci2001.1884

[8] Rorie, R.L., Purcell, L.C., Karcher, D.E., King, C.A. (2011). The assessment of leaf nitrogen in corn from digital images. Crop Science, 51(5): 2174-2180. https://doi.org/10.2135/cropsci2010.12.0699

[9] Kawashima, S., Nakatani, M. (1998). An algorithm for estimating chlorophyll content in leaves using a video camera. Annals of Botany, 81(1): 49-54. https://doi.org/10.1006/anbo.1997.0544

[10] Li, H., Zhang, L., Chen, X., Zhang, Y., Cheng, Y., Hu, C. (2011). Image analysis method in application of digital image on diagnosing wheat nitrogen status. Zhongguo Shengtai Nongye Xuebao/Chinese Journal of Eco-Agriculture, 19(1): 155-159.

[11] Sulistyo, S.B., Woo, W.L., Dlay, S.S. (2018). Ensemble neural networks and image analysis for on-site estimation of nitrogen content in plants. In Proceedings of SAI Intelligent Systems Conference (IntelliSys) 2016: Volume 2, London, United Kingdom, pp. 103-118. https://doi.org/10.1007/978-3-319-56991-8_9

[12] Sulistyo, S.B., Woo, W.L., Dlay, S.S. (2016). Regularized neural networks fusion and genetic algorithm based on-field nitrogen status estimation of wheat plants. IEEE Transactions on Industrial Informatics, 13(1): 103-114. https://doi.org/10.1109/TII.2016.2628439

[13] Cavallo, D.P., Cefola, M., Pace, B., Logrieco, A.F., Attolico, G. (2017). Contactless and non-destructive chlorophyll content prediction by random forest regression: A case study on fresh-cut rocket leaves. Computers and Electronics in Agriculture, 140: 303-310. https://doi.org/10.1016/j.compag.2017.06.012

[14] Barman, U., Choudhury, R.D. (2022). Smartphone image based digital chlorophyll meter to estimate the value of citrus leaves chlorophyll using Linear Regression, LMBP-ANN and SCGBP-ANN. Journal of King Saud University-Computer and Information Sciences, 34(6): 2938-2950. https://doi.org/10.1016/j.jksuci.2020.01.005.

[15] Zhou, L., Yuan, Y., Song, Y., Wang, B. (2017). Research on estimation of wheat chlorophyll using image

processing technology. MATEC Web of Conferences, 128: 01007. https://doi.org/10.1051/matecc onf/201712801007

[16] Yu, Q. (2015). Research on nitrogen nutrition diagnosis of wheat using digital image processing technique. Master's thesis, Nanjing Agricultural University.

[17] Hu, T.Y., Yang, G., Chen, B. (2016). Pearson correlation test-based ARIMA model of displacement prediction. Water Resources and Hydropower Engineering, 47(1): 71-75.

[18] Agarwal, A., Gupta, S.D. (2018). Assessment of spinach seedling health status and chlorophyll content by multivariate data analysis and multiple linear regression of leaf image features. Computers and Electronics in Agriculture, 152: 281-289. https://doi.org/10.1016/j.compag.2018.06.048

[19] Yang, C. (2017). Detection of rape canopy SPAD Based on multispectral images of low altitude remote sensing platform. In 2017 ASABE Annual International Meeting. https://doi.org/10.13031/aim.201700723

[20] Sabouri, H., Sajadi, S.J. (2022). Image processing and area estimation of chia (Salvia hispanica L.), quinoa (Chenopodium quinoa Willd.), and bitter melon (Momordica charantia L.) leaves based on statistical and intelligent methods. Journal of Applied Research on Medicinal and Aromatic Plants, 30: 100382. https://doi.org/10.1016/j.jarmap.2022.100382

[21] Uddin, K., Schofield, J., Widanage, W.D. (2022). State of health estimation of lithium-ion batteries in vehicle-to-grid applications using recurrent neural networks for learning the impact of degradation stress factors. arXiv preprint arXiv:2205.07561. https://doi.org/10.48550/arXiv.2205.07561